

New thick Silicon Carbide detectors: response to 14 MeV neutrons and comparison with single-crystal diamonds

M. Rebai^{1,2}, D. Rigamonti^{1,2}, S. Cancelli³, G. Croci^{2,3}, G. Gorini^{2,3}, E. Perelli Cippo¹, O. Putignano³, M. Tardocchi^{1,2}, C. Altana⁴, M. Angelone⁵, G. Borghi⁶, M. Boscardin⁶, C. Ciampi^{7,8}, G.A.P. Cirrone⁴, A. Fazzi^{9,10}, D. Giove¹⁰, L. Labate¹¹, G. Lanzalone⁴, F. La Via^{12,4}, S. Loreti⁵, A. Muoio⁴, P. Ottanelli^{7,8}, G. Pasquali^{7,8}, M. Pillon⁵, S.M.R. Puglia⁴, A. Santangelo¹³, A. Trifiro^{14,15} and S. Tudisco⁴

¹*Istituto per la Scienza e Tecnologia dei Plasmi Consiglio Nazionale delle Ricerche, Milano, Italy*

²*INFN sezione di Milano-Bicocca, Milano, Italy*

³*Dipartimento di Fisica 'G. Occhialini', Università di Milano-Bicocca, Milano, Italy*

⁴*Istituto Nazionale di Fisica Nucleare (INFN), Laboratori Nazionali del Sud (LNS), Via S. Sofia 62, 95123 Catania, Italy*

⁵*Associazione EURATOM-ENEA sulla Fusione ENEA C.R. Frascati, Via E. Fermi, 45, 00044 Frascati (Roma), Italy*

⁶*Trento Institute for Fundamental Physics and Applications (TIFPA), (INFN), Fondazione Bruno Kessler (FBK-Trento), Via Sommarive 14, 38123 Povo Trento, Italy*

⁷*INFN—Sezione di Firenze, Via G. Sansone 1, 50019 Sesto Fiorentino, Italy*

⁸*Dipartimento di Fisica, Università di Firenze, Via G. Sansone 1, 50019 Sesto Fiorentino, Italy*

⁹*Department of Energy of Politecnico di Milano, Via Lambruschini 4, 20156, Milano*

¹⁰*INFN-Sez Milano, Via Celoria 16, 20133 Milano*

¹¹*Istituto Nazionale di Ottica, Consiglio Nazionale delle Ricerche, Via G. Moruzzi 1, 56124 Pisa, Italy*

¹²*Institute for Microelectronics and Microsystems, Consiglio Nazionale delle Ricerche VIII Strada, 5, 95121 Catania, Italy*

¹³*STMicroelectronics, Stradale Primosole, 50, 95121 Catania, Italy*

¹⁴*Dipartimento di Scienze MIFT dell'Università di Messina, V.le F. S. D'Alcontres 31, 98166 Messina, Italy*

¹⁵*INFN-Sez Catania, Via Santa Sofia, 64 - 95123 Catania*

Abstract

In this work we present the response of a new large volume 4H Silicon Carbide (SiC) detector to 14 MeV neutrons. The device has an active thickness of 100 μm (obtained by epitaxial growing) and an active area of 25 mm^2 . Tests were conducted at the ENEA-Frascati Neutron Generator facility by using 14.1 MeV neutrons. The SiC detector performance was compared to that of Single-Crystal Diamond (SCD) detectors. The SiC response function was successfully measured and revealed a very complex structure due to the presence in the detector of both Silicon and Carbon atoms. Nevertheless, the flexibility in the SiC manufacturing and the new achievements in terms of relatively large areas (up 1x1 cm^2) and a wide range of thicknesses makes them an interesting alternative to diamond detectors in environments where limited space and high neutron fluxes are an issue, i.e. modern neutron cameras or in-vessel tokamak measurements for the new generation fusion machines such as ITER. The absence of instabilities during neutron irradiation and the capability to withstand high neutron fluences and to follow the neutron yield suggest a straightforward use of these detectors as a neutron diagnostics.

1. Introduction

The range of application of high band-gap solid state detectors is expanding in those environments where the high neutron flux is an issue, such as in the high-flux spallation neutron sources and in the thermonuclear fusion environment. An example of the former is the ISIS spallation neutron source (Didcot, U.K.)[1], where neutrons are produced by 800 MeV protons impinging on a heavy material. Being a pulsed neutron source, instant neutron flux can be very high, therefore the small-size and the fast response-time features of high band-gap solid state detectors make them an interesting solution to monitor and measure the neutron flux. Single-crystal Diamond (SCD)

51 detectors have been characterized in the past [2][3][4] and they are currently installed at the Chiplr
52 beam-line at ISIS as beam monitors [5]. Chiplr, built for measuring the Single Events Effects on
53 electronic devices, is a fast neutron beam-line that directly faces the spallation target: the neutron
54 flux exceeds 10^6 n/s/cm² above 10 MeV and therefore dedicated fast-neutron detectors are still in
55 development for the measurement of the neutron flux in the 1-800 MeV energy range and able to
56 work at high rates (> 1 MHz).

57 As for thermonuclear fusion environments, it has been shown that SCDs can be used as excellent
58 spectrometers for 14 MeV neutrons [6] and a SCD detector matrix has been installed, e.g., at JET
59 (Joint European Torus) for the diagnosis of the plasma in the upcoming Deuterium-Tritium campaign
60 [7]. Measurements performed with Deuterium (D) plasmas at JET have demonstrated that
61 spectroscopy with a moderate energy resolution can also be performed [8][9] with 2.5 MeV
62 neutrons. The limited availability of large size commercial single-crystal diamonds has led to the
63 development of a 12-pixel (4.5 x 4.5 mm² each) matrix to boost the counting rate, especially in D
64 plasmas, instead of having a single diamond detector with equal area.

65 Diamond detectors have been shown to withstand neutron fluence up to $2 \cdot 10^{14}$ n/cm² as shown in
66 [10] for single crystal and in [11] for polycrystalline diamonds. The latter, after irradiation with
67 $8 \cdot 10^{14}$ n/cm², recovers up to 70% of their initial performance after a suitable annealing. Moreover,
68 transient effects have been noticed for SCD detectors irradiated with high energy neutrons and
69 alpha particles [13][14]. Transient effects are due to partial trapping of the charge carries within
70 the detector bulk defects and in the interfaces between the diamond crystal and the ohmic contacts.
71 These are known as polarization effects and depend on the type, and amount, of crystal defects,
72 naturally present or induced by neutron irradiation [15][16]. The polarization effect can be reset by
73 inverting the bias voltage, as discussed in [14], but it could affect energy resolution if not accounted
74 for.

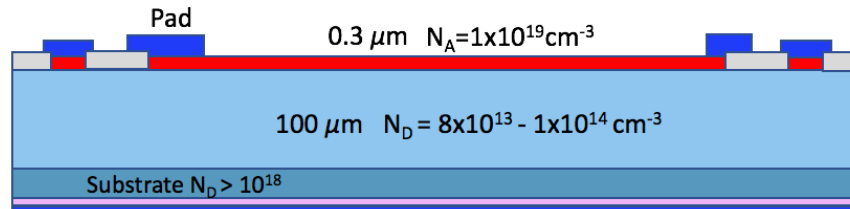
75 In this paper we investigate the performance of new SiC detectors as an alternative to SCDs. SiC
76 devices have been already used in the past to measure the thermal neutron flux in reactors [17] and
77 the 14 MeV neutrons from DT reactions [18]. As shown in [19] good quality SiC detectors are now
78 available and measurement of the fast neutron spectrum is possible also at high temperatures as
79 done with diamond detectors [20].

80 The device used in present work was manufactured by SiCILIA (*Silicon Carbide detectors for Intense*
81 *Luminosity Investigations and Applications*) [21] project which is a collaboration between IMM-CNR
82 and INFN totally funded by INFN. The main goal of the project was the processes innovation and
83 production of relatively large area SiC detectors for many applications [22][23][24][25][26][27], with
84 thicknesses depending on the experiment requirements. Today, thanks to the SiCILIA R&D, SiC can
85 be produced in relatively large areas (up to 1.5 cm²) [28] and with thicknesses up to 250 μ m which
86 represent an excellent enhancement in the SiC growth technology. Moreover in the near future they
87 could be worked in Geiger mode, in order to detect single photons [29][30].

88 Moreover, the possibility of growing SiC layers with large area and with different thickness, makes
89 this material an interesting candidate for applications in fusion plasma physics, like for instance for
90 Fast Ions Loss Detectors (FILD) that measure the fast ions lost by the plasma before they hit the first
91 wall. Currently, FILD systems are based on scintillator crystals coupled to optical fibres leading
92 scintillation light towards a CDD [12]. They work in an environment where neutrons are the highest
93 source of background. An advantage of SiC in this application is that, by decreasing the crystal
94 thickness, the detector efficiency for neutrons can be accordingly decreased to as low as 10^{-5} ,
95 without losing efficiency for 500 keV ions.

96 As in SCDs, neutron detection in SiC is based on the collection of electron-hole pairs produced by
97 charged particles generated by neutron interaction with C and Si nuclei. Due to their abundances in
98 natural C and Si, in this work we will consider only interaction on ¹²C and ²⁸Si. This paper describes

99 measurements performed at the Frascati Neutron Generator (FNG) at Enea (Frascati, Italy) by using
 100 a SiCILIA SiC detector prototype and two SCDs with different thicknesses irradiated by 14 MeV
 101 neutrons. The SiC detector was irradiated up to a total fluence of $4.45 \cdot 10^{11}$ neutrons/cm².
 102 The paper is organized as follows: in Section 2 the neutron-induced reactions on ¹²C and ²⁸Si are
 103 summarized and the detectors are compared in terms of construction parameters and features. In
 104 Section 3 the experiment performed at FNG is described, while in Section 4 the most important
 105 results will be illustrated.



106
 107
 108 **Figure 1** Cross section of the SiC detectors

109 **2. The detectors**

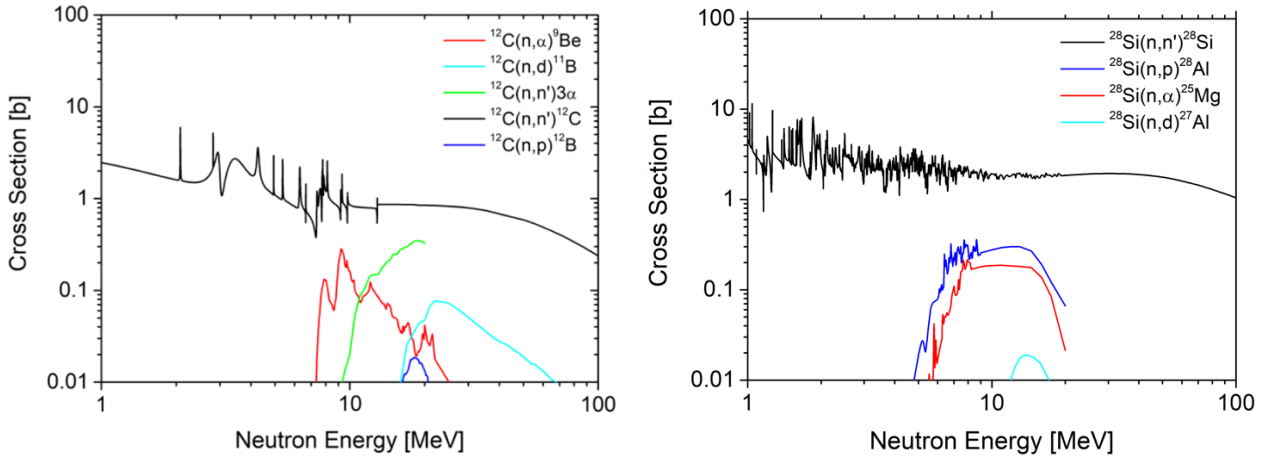
110
 111 *A. Detectors production*

112
 113 The SiC detectors were designed and manufactured at the CNR-IMM (Institute for Microelectronics
 114 and Microsystems) in Catania, starting from the growth of thick 4H epitaxial layers on four inch 4H-
 115 SiC wafers by means of a CVD (Chemical Vapour Deposition) process. During this phase dopants are
 116 provided by means of gaseous precursors such as N₂ for n-type doping and Al₂(CH₃)₆
 117 (Trimethylaluminium) for p-type doping in order to realize p-n junction devices. The process was
 118 performed at a low-pressure and high temperature (1630 °C) regime.

119 The wafers were subsequently treated with several photolithographic steps, a first
 120 photolithography for the definition of the detector area by Inductive Coupled Plasma (ICP) etching
 121 was performed. Then, a second lithography was performed for the construction of the edge
 122 structures, aimed at reducing the electrical field at the device borders. The process continues with
 123 the deposition of an isolation oxide and the opening of the contacts with a further photolithographic
 124 process and a subsequent annealing to perform a good electric contact on p⁺ region. Along the
 125 border of the active area of the detector a 200nm layer of Ti and Al was deposited in order to obtain
 126 a region well-suited for ultrasonic micro-bonding. Finally, the ohmic contact was formed by
 127 Titanium/Nickel/Gold deposition. A cross-section of the SiC detector used for the neutron
 128 measurements described in this paper is shown in Fig.1. It features a 300 nm thick p-layer with a
 129 doping concentration $N_A = 1 \cdot 10^{19} \text{ cm}^{-3}$ and a 100 μm thick n-layer with a doping concentration, N_D ,
 130 between $8 \cdot 10^{13} \text{ cm}^{-3}$ and $1 \cdot 10^{14} \text{ cm}^{-3}$. The detector has an active area of about 10x10 mm²,
 131 segmented in four regions of 5x5 mm², and was mounted on a PCB board (Figure 3 A) designed to
 132 be housed in an aluminium box.

133 The SCD detectors were designed and built at the CNR-IFP (Institute of Plasma Physics) in Milan and
 134 at the CNR-ISM institute in Rome (Italy) [31][32][33]. The first SCD is made of a single-crystal
 135 diamond sample (4.5x4.5x0.5mm³) grown with a CVD technique with boron concentration [B] <5
 136 ppb and nitrogen concentration [N] <1 ppb), provided by Element Six Ltd. [34]. The second, equal
 137 to the first one, has been thinned by laser cutting to a layer thickness of 150 μm. Ohmic contacts
 138 were obtained on the top and bottom surfaces of the samples by subsequent sputtering depositions
 139 of a multilayer metal structure (patent pending), followed by a final gold layer deposition, in order
 140 to improve weldability with microwires and to prevent oxidation of the underlying structure. The

141 contact thickness is 200 nm with a lateral dimension of $4.2 \times 4.2 \text{ mm}^2$. A dedicated 1mm thick alumina
 142 Printed Circuit Board (PCB) was designed and fabricated; the bottom surfaces of the diamond
 143 samples were glued with a thin layer of conductive silver paste on the pad, whereas the top surfaces
 144 were wire-bonded (by means of $25 \mu\text{m}$ thick Al/Si wires) on the ground plane. The alumina PCB is
 145 housed inside a properly designed aluminium metal case in order to shield it from electromagnetic
 146 interference and to give the detectors the mechanical resistance necessary for handling.
 147



148
 149 **Figure 2** Cross sections for neutron interaction on Carbon (left) and on Silicon (right). Data from the ENDF/B-VI.0 for ^{12}C and
 150 ENDF/B-VIII.0 for ^{28}Si [35].

151
 152 **A. Neutron detection**

153
 154 Neutron detection is based on the collection of the electron-hole (e-h) pairs produced by neutron
 155 interaction with ^{12}C in SCDs and with both ^{12}C and ^{28}Si in SiC detectors. The most important reactions
 156 induced by neutrons in the MeV energy range on Carbon and Silicon are reported in Table 1 and
 157 their cross-sections in Figure 2. The most relevant neutron-induced process in both Carbon and
 158 Silicon is the *elastic scattering* (black lines in Figure 2), in which only a fraction of the neutron energy
 159 is released into the detector, by means of the energy of the recoiling atom, given by
 160 $E_d = E_n \cdot \cos^2(\theta) / (1 + A)^2$, where E_n is the incoming neutron energy, θ is the recoil angle and A the
 161 mass number of the recoiling atom. The maximum energy that can be released into the detector is
 162 $E_{d,\text{max}} = 4.00 \text{ MeV}$ and $E_{d,\text{max}} = 1.87 \text{ MeV}$ for recoils of Carbon and Silicon ions, respectively. All the
 163 energy values smaller than $E_{d,\text{max}}$ can possibly be released by this process into the detector; as a
 164 consequence, a typical edge-type shape is produced into the Pulse Height Spectrum (PHS) of the
 165 detector. Concerning the reactions $^A\text{X}(n,\alpha)^{A-3}\text{Y}$ and $^A\text{X}(n,p)^{A-1}\text{Y}$, being two-body reactions, all the
 166 neutron energy minus the reaction Q-value is deposited into the detector.
 167

168 **Table 1:** Main 14 MeV neutron-induced reactions on Carbon and Silicon. For each reaction, the threshold, the Q-value and the
 169 position of the peak in the PHS are given. The last column is the label of the peak observed in the experimental PHS shown in **Figure**
 170 **6.** If the nucleus is left in an excited state the energy which can be released into the detector is given for the first nine excited states.

| Reaction | Threshold | Q _{value} [MeV] | E _d [MeV] | Label |
|--------------------------------------|-------------------|--------------------------|------------------------|-------|
| $^{12}\text{C}(n,n)^{12}\text{C}$ | - | - | $E_{d,\text{max}}=4.0$ | 0 |
| $^{12}\text{C}(n,\alpha)^9\text{Be}$ | 6.2 | -5.702 | | |
| | Ground state | | 8.398 | 1 |
| | 1st excited state | | 6.761 | |
| $^{12}\text{C}(n,p)^{12}\text{B}$ | 13.645 | -12.587 | | |
| | Ground state | | 1.513 | |
| | 1st excited state | | 0.56 | |

| | | | | |
|--------------------------------------------|-------------------|--------|-------------------------|----|
| $^{12}\text{C}(n,n')3\alpha$ | 7.886 | -7.275 | 6.825 | 2 |
| $^{28}\text{Si}(n, n) ^{28}\text{Si}$ | - | - | $E_{d,\text{max}}=1.87$ | |
| $^{28}\text{Si}(n, \alpha) ^{25}\text{Mg}$ | Ground state | | 11.446 | 3a |
| | 1st excited state | | 10.861 | 3b |
| | 2nd excited state | | 10.471 | 3c |
| | 3rd excited state | | 9.834 | 3d |
| | 4th excited state | | 9.481 | 3e |
| | 5th excited state | | 8.644 | 3f |
| | 6th excited state | | 8.041 | 3g |
| | 7th excited state | | 8.032 | 3h |
| | 8th excited state | | 7.538 | 3i |
| | 9th excited state | | 7.475 | 3j |

171

172

173

174

3. Experimental set-up

175

176

177

178

179

180

181

182

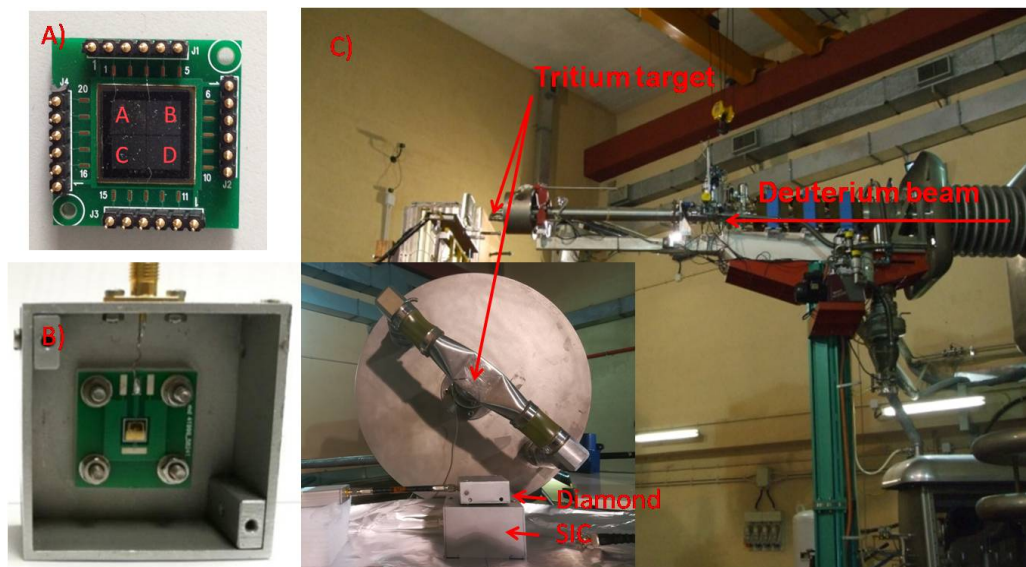
183

184

185

The response function of both SCDs and of the SiC detector, together with their neutron resistance and stability, has been investigated by irradiating the detectors with 14.1 MeV neutrons at FNG. Here, neutrons are produced by Deuterium-Tritium (DT) reactions obtained from deuterium ions accelerated up to 300 keV impinging on a tritiated-titanium target [36]. The detectors were placed at 90 degrees with respect to the beam direction (see Figure 3) at a distance between 13 and 18 cm from the target. The expected neutron spectrum at the detector position, calculated through MCNP simulations [37], features a main component, peaked at 14.1 MeV with a 130 keV broadening and a scattered neutron component at lower energies (see Figure 4).

During the measurements, the FNG neutron yield has been monitored as a function of time by the standard FNG monitor which detects the alpha particles produced by the DT reactions in the target.



186

187

188

Figure 3 Pictures of the Silicon Carbide (A) and Single-crystal Diamond (B) detectors and their installation at the FNG facility (C). The SiC detector used for the measurement was the one labelled "A" in the top left panel.

189

190

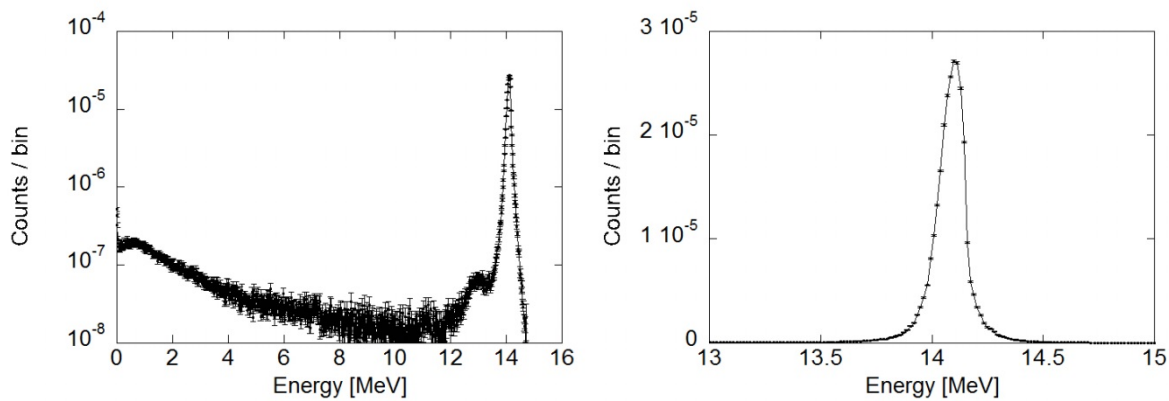
191

192

193

A dedicated custom electronic chain was used to bias and collect charge carriers from each detector. In particular, the SCDs were coupled (through a 5 cm RG62 cable) to a CIVIDEC C6 fast charge preamplifier [38] with rise time of 3.5 ns and a shaping time of 25 ns. Signals were directly fed into a CAEN DT5730B digitizer (500 MSample/s and 14 bits) equipped with CAEN software able to perform on-line measurements of the pulse area [39].

194 The SiC spectrometer was connected to an ORTEC 142A preamplifier [40] with nominal decay time
 195 of 500 μ s; the signal from it was fed into an ORTEC 570 amplifier [40] which provided a gain factor
 196 of 1000 and a shaping time of 1 μ s. Finally, the signal was recorded and analysed in amplitude by a
 197 MAESTRO multi-channel analyser (MCA) [40]. Alternatively, for some measurements, the SiC was
 198 preamplified by a CX-L CIVIDEC spectroscopic amplifier producing a Gaussian output signal of 180
 199 ns FWHM [38] and then directly digitized by the CAEN DT5730B.
 200 Both the SCDs and the SiC detectors were biased by a CAEN NDT1470 [39] HV Module. A bias voltage
 201 V_{bias} equal to +400V and +120V was used to polarize the 500 μ m and the 150 μ m thick SCDs,
 202 respectively, giving rise to a constant electric field in the whole SCDs bulk of 0.8V/ μ m. A V_{bias} equal
 203 to -400V was used to polarize the SiC creating a depletion region of 73 μ m.



204 **Figure 4** FNG Neutron spectrum expected at the SiC position. The spectrum, reported in logarithmic (left) and linear (right) scale, is
 205 peaked at 14.1 MeV with a 130 keV broadening.
 206

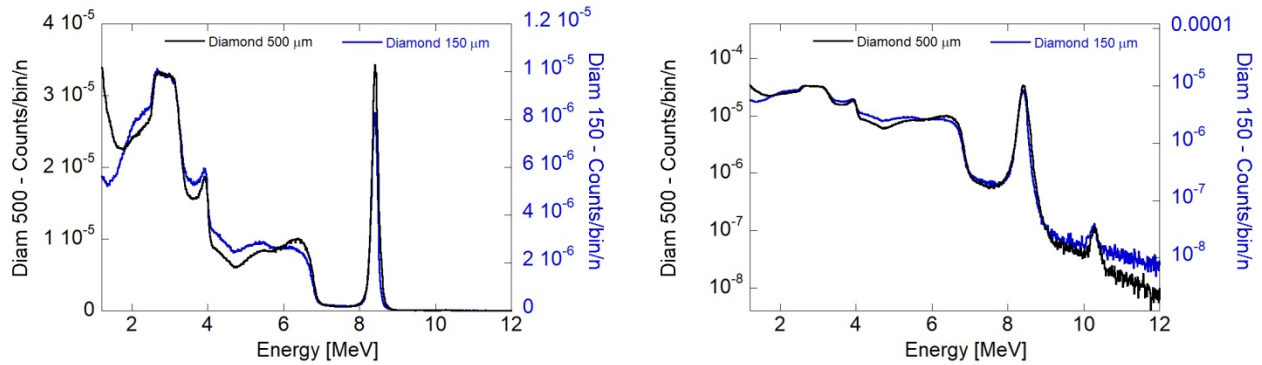
207 4. Measurements with 14 MeV neutrons

208 The PHS measured with the two SCDs (Figure 5) feature the characteristic structures of neutron
 209 interaction with Carbon described in Section 2. A prominent peak, due to the $^{12}\text{C}(n,\alpha)^9\text{Be}$ reaction,
 210 is clearly visible at 8.4 MeV. This peak features a FWHM of 203 keV and 191 keV for the two SCDs
 211 (500 and 150 μ m), respectively: taking into account the 130 keV FWHM of the beam, an energy
 212 resolution of 1.84% and 1.67% for the 500 μ m and the 150 μ m diamond has been obtained,
 213 respectively. At lower energies, three edges can be observed. The one at 6.8 MeV is due the carbon
 214 break-up reaction into three α particles, $^{12}\text{C}(n,n')3\alpha$. The edge at 4 MeV is due to the elastic recoil
 215 on ^{12}C , while the structure between 2.7 MeV and 3.3 MeV is due to a combination of *i*) elastic recoil
 216 at higher recoiling angles, *ii*) elastic recoil leaving carbon in the first excited state and *iii*) the carbon
 217 break-up reaction. Although, the two SCDs show a very similar PHS shape, a clear discrepancy
 218 between the two SCDs is observed in the lower energy part of the spectrum. This discrepancy, also
 219 visible in the (n,α) peak, is still under investigation and it could be due to the “wall” effect [41]
 220 related to the different diamond thickness.

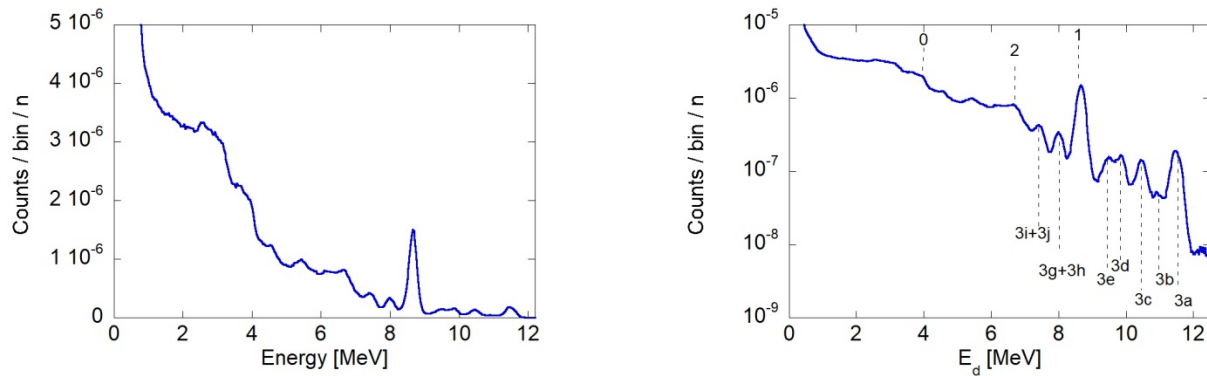
221 If the PHS are observed in logarithmic scale, a peak at 10.3 MeV is clearly visible above the
 222 background. This peak is due to the $^{13}\text{C}(n,\alpha)^{10}\text{Be}$ reaction, which has a lower Q-value (-3.83 MeV)
 223 with respect to the (n,α) reaction on ^{12}C . Its intensity is limited to 0.5% of the (n,α) peak on ^{12}C
 224 by both its lower cross-section and the low natural abundance of ^{13}C (1.1%). These events limit the
 225 SCDs sensitivity on the high energetic ions in DT plasmas to about 10^{-2} with respect to main bulk
 226 emission as mentioned in [42].

227 The SiC PHS shows a more complicated structure due to the presence of the ^{28}Si , in particular,
 228 neutron interaction via (n,α) and (n,p) reactions on ^{28}Si can leave the ^{25}Mg and ^{28}Al nuclei on either
 229
 230

231 the ground state or the first excited states with different finite probabilities. This results in a number
 232 of peaks in the PHS that, together with the neutron-induced reactions on ^{12}C , give the spectra in
 233 Figure 6. The most important structures in the PHS have been labelled as in Table 1 in order to
 234 improve the comprehension of the spectrum. The most intense peak is placed at $E_d=8.4$ MeV and it
 235 is related to the (n,α) reaction on ^{12}C on the ground state. The same reaction channel on ^{28}Si can be
 236 observed at $E_d=11.4$ MeV. The intensity of this peak is limited with respect to the one occurring on
 237 ^{12}C because the (n,α) reaction can produce ^{25}Mg in an excited energy level (contributions
 238 corresponding to excited levels up to the 9th can be recognized in Fig.6).
 239



240 **Figure 5** PHS for the 150 μm thick diamond (blue line) and the 500 μm thick diamond (black line) in linear (left) and log scale (right).
 241 The left Y-axis refers to the spectrum obtained with the 500 μm SCD, while the right one refers to the 150 μm thick SCD. The spectra
 242 have been normalized with respect to the neutron fluence ($1.1 \pm 0.2 \cdot 10^{10} \text{ n/cm}^2$ for the 500 μm diamond $2.6 \pm 0.4 \cdot 10^{10} \text{ n/cm}^2$ for the
 243 150 μm diamond) and to the bin width is equal to 22 keV.
 244



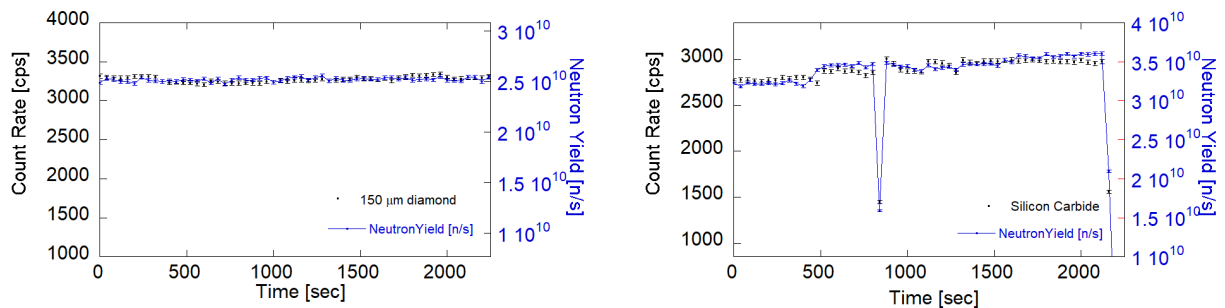
245 **Figure 6** Pulse Height spectrum for the SiC in linear and log scale obtained with the ORTEC 142A preamplifier and 570 amplifier. The
 246 spectra have been normalized with respect to the neutron fluence ($2.4 \pm 0.3 \cdot 10^{10} \text{ n/cm}^2$) and the bin width is 22 keV. The labels in
 247 the log scale spectrum refer to the different reactions summarized in **Table 1**.
 248

249
 250 At lower deposited energies the elastic edge on ^{12}C , placed at $E_d=4$ MeV is still visible, but the same
 251 interaction channel on ^{28}Si , which should be placed at 1.87 MeV, cannot be distinguished from the
 252 background. The (n,α) peaks feature a FWHM of 265 keV for the reaction $^{12}\text{C}(n,\alpha)^9\text{Be}$ and 365 keV
 253 for $^{28}\text{Si}(n,\alpha)^{25}\text{Mg}$ when ^{25}Mg is produced in the ground state: taking into account the beam energy
 254 FWHM of 130 keV, an energy resolution of 2.7% and 3% has been obtained respectively for the two
 255 peaks. The energy resolution achieved is good enough for measuring the temperature in ohmic
 256 plasmas [43] where an energy resolution better than 5% is required.
 257 Besides the energy resolution and the sensitivity of the (n,α) peak to high energy components of
 258 the neutron spectrum, a crucial feature for neutron detectors is their efficiency. Two parameters

259 can be used to assess the efficiency: the overall counts above a certain energy threshold and the
 260 counts corresponding to a specific reaction channel. Both methods have been used in this work. The
 261 threshold used for the evaluation of the efficiency has been chosen equal to $E_d=1.2$ MeV for all the
 262 detectors in order to discard the gamma-ray background and the counts due to electronic noise.
 263 The reaction channel used to compare the efficiency is the $^{12}\text{C}(n,\alpha)^9\text{Be}$ reaction producing the only
 264 peak in common between the two kind of detectors. The measured efficiency is here compared with
 265 the results of GEANT4 simulations giving the results shown in shown in Table 2.
 266

| Detector | Atomic/ molecular density [cm^{-3}] | Detector volume [cm^3] | Efficiency measured for $E_d >$ 1.2 MeV [and normalized per atom] | Simulated efficiency for $E_d >$ 1.2 MeV [and normalized per atom] | Efficiency measured in the $^{12}\text{C}(n,\alpha)^9\text{Be}$ peak | Simulated efficiency in the $^{12}\text{C}(n,\alpha)^9\text{Be}$ peak |
|--------------------------|---------------------------------------------------------|-----------------------------------------|-------------------------------------------------------------------------------|--------------------------------------------------------------------------------|----------------------------------------------------------------------------|-----------------------------------------------------------------------------------|
| SCD 500 μm | $1.76 \cdot 10^{23}$ | $1.0125 \cdot 10^{-2}$ | $(5.32 \pm 0.87) \cdot 10^{-3}$ [$2.98 \cdot 10^{-24}$] | $5.2 \cdot 10^{-3}$ [$2.92 \cdot 10^{-24}$] | $(3.98 \pm 0.73) \cdot 10^{-4}$ | $5.45 \cdot 10^{-4}$ |
| SCD 150 μm | $1.76 \cdot 10^{23}$ | $3.0375 \cdot 10^{-3}$ | $(1.59 \pm 0.25) \cdot 10^{-3}$ [$2.97 \cdot 10^{-24}$] | $1.6 \cdot 10^{-3}$ [$2.99 \cdot 10^{-24}$] | $(0.91 \pm 0.15) \cdot 10^{-4}$ | $1.47 \cdot 10^{-4}$ |
| SiC 100 μm | $4.8 \cdot 10^{22}$ | $2.5 \cdot 10^{-3}$ | $(5.69 \pm 0.78) \cdot 10^{-4}$ [$4.74 \cdot 10^{-24}$] | $6.73 \cdot 10^{-4}$ [$5.61 \cdot 10^{-24}$] | $(2.02 \pm 0.30) \cdot 10^{-5}$ | $2.73 \cdot 10^{-5}$ |

267
 268 **Table 2** Efficiency measured and simulated for the three detectors for $E_d > 1.2$ MeV and in the $^{12}\text{C}(n,\alpha)^9\text{Be}$ peak (note that for $E_d > 1.2$
 269 MeV the efficiency per atom is reported in square brackets). The error on the measured efficiency is the combination of the statistic
 270 error, a 5% uncertainty on the measure of the neutron fluence and a 5% uncertainty due to the subtraction of the background.
 271 Together with the values of the efficiency the detector volume and atomic/molecular density are reported.



272
 273 **Figure 7** 150 μm diamond (left) and SiC (right) detector counting rate compared to FNG neutron yield, both binned every 40 seconds.
 274 Note that the plots are in double Y scale: the left axis refers to the detectors counting rate while the right one refers to the neutron
 275 yield. The scale ratio between Y_{max} and Y_{min} is equal to 4 for all the plots.

276
 277 The most efficient detector among the ones examined is the 500 μm -thick diamond; this is due to
 278 the fact that the probability of neutron interaction scales with the volume of the detector and the
 279 material atomic density. The agreement between the simulated and the measured efficiency is
 280 rather good in all the considered cases especially for the overall efficiency. Moreover, the efficiency
 281 normalized to atom number indicates that the two SCD detectors behave the same when irradiated
 282 with fast neutrons; on the other hand, the higher normalized efficiency of the SiC reflects the higher
 283 neutron reaction cross section on Silicon.

284 The measured efficiency for the $^{12}\text{C}(n,\alpha)^9\text{Be}$ peak is always lower than the simulated one. This could
 285 be due to events with only a partial charge collection efficiency not contributing to the main peak.

286 It could also be due to discrepancies between the $^{12}\text{C}(n,\alpha)^9\text{Be}$ reaction cross section employed in
287 the simulation and the actual one.

288 Together with the efficiency evaluation, the stability of the detectors compared to the total FNG
289 neutron yield was measured. The FNG neutron yield, monitored during the irradiation of all the
290 detectors, showed a very good agreement in terms of counting rate with all the detectors (Figure
291 7). The Pearson correlation coefficients were calculated for the two detectors being equal to 0.9793
292 and 0.9770 for the diamond and the SiC respectively.

293

294

295 5. Conclusion

296

297

298 The Silicon Carbide detector produced within the SiCILIA project has been tested at FNG by using
299 14.1 MeV neutrons. The detector, featuring an active area of 25 mm^2 and an epitaxial thickness of
300 $100\text{ }\mu\text{m}$, showed good efficiency values thus demonstrating the improvements made in the growing
301 procedures. The absence of instabilities during neutron irradiation up to a 14 MeV neutron fluence
302 of $4.45 \cdot 10^{11}\text{ n/cm}^2$ suggests a straightforward use of this detector as a fast neutron diagnostic. The
303 Pulse Height spectrum obtained from the SiC detector revealed a very complex response function
304 due to the presence of both ^{12}C and ^{28}Si . This complexity limits the sensitivity of the SiC when used
305 as a neutron spectrometer for Deuterium-Tritium plasma diagnostics [7][42], though it could be well
306 suited to measure the temperature in thermal plasmas. Furthermore, it could be successfully used
307 as a neutron diagnostic in those environments in which small size is a requirement, such as in a
308 neutron camera. In addition, the possibility of growing Silicon Carbide layers with different
309 thicknesses allows for tuning the neutron detection efficiency, and, therefore, using SiC crystals as
310 charged particle detectors in those environments where high neutron fluxes are an issue, such as in
311 FILD detectors.

312 This work is the first step towards the realization of a fast neutron detector based on Silicon Carbide.
313 More measurements are planned in order to measure the SiC detector response function to
314 neutrons of different energies as already done for diamond based detectors [45] and to assess the
315 detector radiation hardness as done in [10] with diamonds. The present work shows that the Silicon
316 Carbide detector is able to withstand 14 MeV neutron irradiation without changing its performances
317 which is of particular relevance in the case of the future nuclear fusion machines, such as ITER [46].

318

319

320

321 Acknowledgments

322

323 The work leading to this publication was funded by the INFN-Group 5 (Technology Research) and
324 by EuroFusion-WP-JT60SA. The views and opinions expressed herein do not necessarily reflect those
325 of Eurofusion and INFN.

326

327 References

- 328 [1] <https://www.isis.stfc.ac.uk/>
329 [2] M. Rebai et al., Journ. of Instrum 7 C05015 (2012). doi:10.1088/1748-0221/7/05/C05015
330 [3] M. Rebai et al., Nucl. Phys B 215, 313-315, 2011; doi:10.1016/j.nuclphysbps.2011.04.041
331 [4] C. Cazzaniga et al., JINST 11 P07012 (2016)
332 [5] C. Cazzaniga and C. D. Frost, Journal of Physics: Conference Series, Vol. 1021, conference
333 [6] D. Rigamonti et al., Meas. Sci. Technol. 29 045502

334 [7] L. Giacomelli et al., Rev. Sci. Instrum 87, 11D822 (2016); doi: 10.1063/1.4960307.
335 [8] M. Rebai et al., Rev. Sci. Instrum. 87, 11D823 (2016); doi: 10.1063/1.4960490
336 [9] A. Muraro et al., Rev. Sci. Instrum 87, 11D833 (2016); doi: 10.1063/1.4961557
337 [10] M. Pillon et al., Journal of Applied Physics 104, 054513 (2008)
338 [11] M. Angelone et al., Rev. Scient. Instrum 77, 023505 (2006)
339 [12] M. García-et al, Nucl. Fus. 47, 7 (2007)
340 [13] C. Cazzaniga et al., Nuclear Inst. and Methods in Physics Research, B 405 (2017) 1-10
341 [14] M. Rebai et al., Diamond & Related Materials 61 (2016) 1–6, DOI: 10.1016/j.diamond.2015.11.002
342 [15] Tanaka T. Tanaka et al., Diamond & Related Materials 14 (2005), 2031 -2034
343 [16] A. Lohstroh et al., Diamond & Related Materials 19 (2010) 841-845
344 [17] Frank H. Ruddy, et al., (2002) Radiation Detectors, Nuclear Technology, 140:2, 198-208
345 [18] Frank H. Ruddy, et al., IEEE TRANSACTIONS ON NUCLEAR SCIENCE, VOL. 53, NO. 3, JUNE 2006
346 [19] D. Szalkai, et al., Animma2015-283
347 [20] M. Angelone et al., (2017) 2016 IEEE Nuclear Science Symposium, Medical Imaging Conference and Room-
348 Temperature Semiconductor Detector Workshop, NSS/MIC/RTSD 2016, 2017-January, art. no. 8069929
349 [21] A. Muoio et al., Eur. Phys. Jour., Web of Confer. 117, UNSP 10006 (2016)
350 [22] D. Carbone et al. Jour. of Phys. Conf. 312, 082016 (2011)
351 [23] G. Cristoforetti et al. Plasma Phys. and Contr. Fus. Vol. 56, iss. 9, n° 095001 (2014)
352 [24] D. Mascali et al. Rad. Eff. And Def. in Sol., 165, 730-736 (2010)
353 [25] D. Mascali et al. Eur. Phys. Lett., 100, 45003 (2012)
354 [26] L. Lanzaò et al. Euro. Biophys. Jour. with Biophys Lett., 36, 823-829 (2007)
355 [27] M. Lacognata et al. Phys. Lett. B, 664, 157-161 (2008)
356 [28] S. Tudisco et al., Sensors, 18, 2289 (2018)
357 [29] M. Mazzillo et al. Sens. and Actuators A-Phys, 138 306-312 (2007)
358 [30] P. Finocchiaro et al. Jour. of Mod. Optics, 54 199-212 (2007)
359 [31] D. M. Trucchi, et al.,IEEE Electron Device Lett. 33, 615–617 (2012)
360 [32] M. Girolami et al., IEEE Electron Device Lett. 33, 224–226 (2012).
361 [33] D. M. Trucchi et al., Diamond Relat. Mater. 14, 575–579 (2005).
362 [34] See <http://www.e6.com> for Element Six Ltd.
363 [35] <https://www-nds.iaea.org/exfor/exfor.htm>
364 [36] M. Angelone et al., Rev. Sci. Instrum. 67 (1996) 2189]
365 [37] <https://mcnp.lanl.gov/>
366 [38] www.cividec.at
367 [39] www.caen.it
368 [40] www.ortec-online.com
369 [41] G.F. Knoll, "Radiation detection and measurement"
370 [42] C. Cazzaniga et al., Rev. of Sci. Instrum. 85, 11E101 (2014); doi: 10.1063/1.4885356
371 [43] W. R. Faust and E. G. Harris, Nucl. Fusion 1, 62 (1960).
372 [44] C. Cazzaniga et al., Rev. of Sci. Instrum. 85, 043506 (2014); doi: 10.1063/1.4870584
373 [45] M. Rebai et al., Journal of Instrum 8 P10007 (2013); doi:10.1088/1748-0221/8/10/P10007
374 [46] <https://www.iter.org/>